INTERNATIONAL JOURNAL FOR NUMERICAL AND ANALYTICAL METHODS IN GEOMECHANICS, VOL. 22, 263–275 (1998)

SCATTERING OF ELASTIC WAVES BY A PLANE CRACK OF FINITE WIDTH IN A TRANSVERSELY ISOTROPIC MEDIUM

J. M. CARCIONE*

Osservatorio Geofisico Sperimentale, P.O. Box 2011 Opicina, 34016 Trieste, Italy

SUMMARY

This work presents a numerical algorithm for solving crack scattering in a transversely isotropic medium whose symmetry axis is perpendicular to the crack surface. The crack is modelled as boundary discontinuities in the displacement u and the particle velocity v, of the stresses $[\kappa u + \zeta v]$, where the brackets denote discontinuities across the interface. The specific stiffness κ introduces frequency-dependence and phase changes in the interface response and the specific viscosity ζ is related to the energy loss.

The numerical method is based on a domain decomposition technique that assignes a different mesh to each side of the interface, that includes the crack plane. As stated above, the effects of the crack on wave propagation are modelled through the boundary conditions, that require a special boundary treatment based on characteristic variables. The algorithm solves the particle velocity–stress wave equations and two additional first-order differential equations (two-dimensional case) in the displacement discontinuity. For each mesh, the spatial derivatives normal to the interface are solved by the Chebyshev method, and the spatial derivatives parallel to the interface are computed with the Fourier method. They allow a highly accurate implementation of the boundary conditions and computation of the spatial derivatives, and an optimal discretization of the model space. Moreover, the algorithm allows general material variability.

Int. J. Numer. Anal. Meth. Geomech., Vol. 22, 263–275 (1998)

Key words: non-ideal interface; crack scattering; domain decomposition; collocation methods

1. INTRODUCTION

The study of crack scattering plays an important role in seismology, exploration geophysics and material science: cracks and fractures in the Earth's crust[1] may constitute possible sources of earthquakes, and hydrocarbon and geothermal reservoirs are mainly composed of partially saturated cracks and microcracks[2]; moreover, ultrasonic waves are used to detect flaws and cracks in order to prevent material failure.[3]

Simulation of crack scattering requires a suitable interface model for describing the dynamic response of the crack surface. Theories that consider imperfect contact were mainly based on the displacement discontinuity model at the interface. Recently, Pyrak-Nolte *et al.*[1] proposed a non-welded interface model based on the discontinuity of the displacement and the particle

[1]Correspondence to: J. M. Carcione, Osservatorio Geofisico Sperimentale, P.O. Box 2011 Opicina, 34016 Trieste, Italy, E-mail: carcione@gems755.ogs.trieste.it.

CCC 0363–9061/98/040263–13$17.50

Received 3 April 1996
Revised 11 July 1997

velocity across the interface. The stress components are proportional to the displacement and velocity discontinuities through the specific stiffnesses and a specific viscosity, respectively. Displacement discontinuities conserve energy and yield frequency-dependent reflection and transmission coefficients. On the other hand, velocity discontinuities imply an energy loss at the interface and frequency-independent reflection and transmission coefficients. The specific viscosity accounts for the presence of a liquid under saturated conditions. The liquid introduces a viscous coupling between the two surfaces of the fracture[4] and enhances energy transmission, but at the same time this is reduced by viscous losses. The model is phenomenological and may account for some slip and dilatancy effects as those described, for instance, by a recent interface model proposed by Mroz and Giambianco.[6]

Elastic wave scattering by a circular crack in a transversely isotropic solid was investigated by Kundu and Boström.[5] They used an analytical solution method and considered stress-free boundary conditions at the interface, implying a complete decoupling of the two surfaces which corresponds to zero stiffnesses and zero specific viscosity.

In this work, we consider a time-domain model to account for displacement and particle velocity discontinuities at the interface. The imperfect bonding is described by four parameters: the normal and tangential specific stiffnesses and viscosities. The stiffnesses account for frequency-dependent and phase-change effects, and the viscosities allow for damping in the interface response. In order to model a crack embedded in a finely laminated background, we assume that this is described by a transversely isotropic medium whose symmetry axis is perpendicular to the crack surface and to the free surface. For instance, composite materials or geological layers whose stratification plane is parallel to the Earth's surface. Note that the equivalence between a laminated medium and a transversely isotropic medium holds when the dominant wavelength of the signal is long compared to the thickness of the layers.

The elastodynamic equations are given in the velocity–stress formulation and the crack equations are two first-order differential equations in the normal and tangential displacement discontinuities. The numerical algorithm is based on a domain decomposition technique,[7] where the implementation of the boundary conditions requires a special treatment based on characteristic variables.[8] Then, the governing equations are solved by a grid method that uses the Chebyshev differential operator normal to the interface, and the Fourier differential operator in the direction parallel to the interface.

2. THE INTERFACE MODEL AND NUMERICAL MODELLING TECHNIQUE

Consider a planar crack of finite width embedded in an elastic and transversely isotropic homogeneous medium. That is, the material on both sides of the crack (two media formally) is the same. The non-ideal characteristics of the crack surface are modelled through the boundary conditions. If the displacement and stress field are continuous across the interface (ideal or welded contact), the reflection coefficient is zero and the interface cannot be detected. On the other hand, if the two media are in non-ideal contact, reflected waves with appreciable amplitude can exist.

The model proposed here is based on the discontinuity of the displacement and particle velocity fields across the interface. We consider the two-dimensional case, and refer to the upper and lower media with the labels I and II, respectively, with z increasing toward the upper medium (see Figure 1). Then, the boundary conditions for a wave impinging on the interface ($z = 0$) are

$$\kappa_x[u_x] + \zeta_x[v_x] = \sigma_{xz} \tag{1}$$

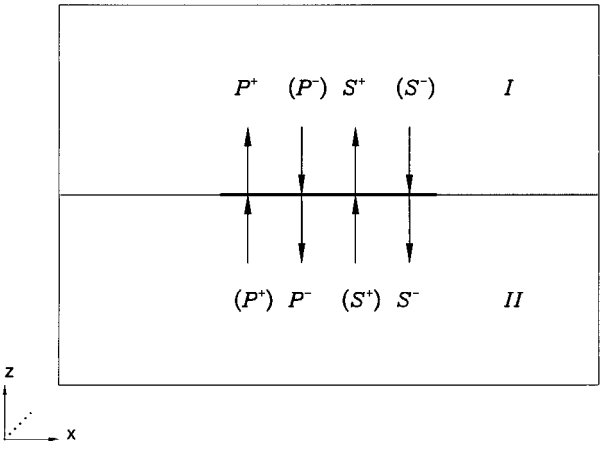

Figure 1. Diagram showing a crack between media I and II. The algorithm uses a domain decomposition technique based on characteristics variables. The incoming variables (in parenthesis) are calculated from the boundary conditions that define the type of crack

$$\kappa_z[u_z] + \zeta_z[v_z] = \sigma_{zz} \tag{2}$$

$$[\sigma_{xz}] = 0 \tag{3}$$

$$[\sigma_{zz}] = 0 \tag{4}$$

where t is the time variable, u_x and u_z are the displacement components, v_x and v_z are the particle velocity components, σ_{xz} and σ_{zz} are the stress components, $\kappa_x(x)$ and $\kappa_z(x)$ are specific stiffnesses and $\zeta_x(x)$ and $\zeta_z(x)$ are specific viscosities. They have dimensions of stiffness and viscosity per unit length, respectively. Moreover, the brackets denote discontinuities across the interface, such that for a field variable ϕ, it is $[\phi] = (\phi)_{\mathrm{II}} - (\phi)_{\mathrm{I}}$.

The model simulates the crack by a zero width layer of distributed spring-dashpots. It can be shown that relaxation-like functions of Maxwell type govern the tangential and normal coupling properties of the crack. The interface exhibits time-dependent mechanical properties through the relaxation functions, and, as in a viscoelastic material, this implies energy dissipation. The boundary conditions (1)–(4) are analysed in Appendix I by a plane wave analysis for normal incidence. A displacement discontinuity ($\kappa_z \neq 0$) yields a change of phase, while a discontinuity in the particle velocity ($\zeta_z \neq 0$) implies an energy loss at the interface.

A similar model, based on combined displacement and velocity discontinuities, was developed by Pyrak-Nolte *et al.*,[1] who introduced a single parameter (η) to describe the viscous coupling between the two surfaces of a fracture. Note that $\kappa_i = 0$ gives the displacement discontinuity model and $\zeta_i = 0$ gives the particle velocity discontinuity model. On the other hand, if $\zeta_i \to \infty$, the model gives the ideal (welded) interface.

The characteristics of the medium are completed with the constitutive relations. The interface equations (1) and (2) can be implemented in a numerical solution algorithm based on a particle velocity–stress formulation yielding a first-order differential equation in the displacement discontinuities that must be solved simultaneously with the equations of momentum conservation.

The interface model is implemented in numerical modelling by using a domain decomposition technique.[7, 9] The boundary treatment is based on characteristics representing one-way waves propagating with the phase velocity of the medium. The wave equation is decomposed into outgoing and incoming wave modes perpendicular to the interface separating the two media (see Figure 1). The outgoing waves are determined by the solution inside the corresponding medium, while the incoming waves are calculated from the boundary conditions.

The particle velocity–stress equation and the interface equations are solved by a fourth-order Runge–Kutta time integration algorithm. The spatial derivatives of the field variables are computed by using the Fourier method in the horizontal direction, and the Chebyshev method in the vertical directions, where non-periodic boundary conditions are required. For instance, Figure 2 illustrates a typical mesh system where the collocation (grid) points can be appreciated. Along the horizontal direction the coordinates of the sampling points are given by

$$x_j = \frac{x_{\max}}{N_x}(i-1), \quad i = 1, \ \ldots, N_x \tag{5}$$

where $x_{\max}$ is the maximum distance and N_x is the number of grid points. For a given function $f(x)$, with transform $\tilde{f}(k_x)$, derivatives are computed as

$$\frac{\tilde{\partial} f}{\partial x} = \imath k_x \tilde{f} \tag{6}$$

where k_x is the discrete wave number and $\imath = \sqrt{-1}$.

On the other hand, the conventional Chebyshev differential operator requires time steps of the order $O(N_z^{-2})$, where N_z is the vertical number of grids points. In order to use time steps of order $O(N_z^{-1})$, which are those required by the Fourier method, the vertical sampling points are defined by

$$z_i = g(\zeta_i), \quad \zeta_i = \cos\left(\frac{\pi i}{N_z}\right), \quad i = 0, \ \ldots, N_z - 1 \tag{7}$$

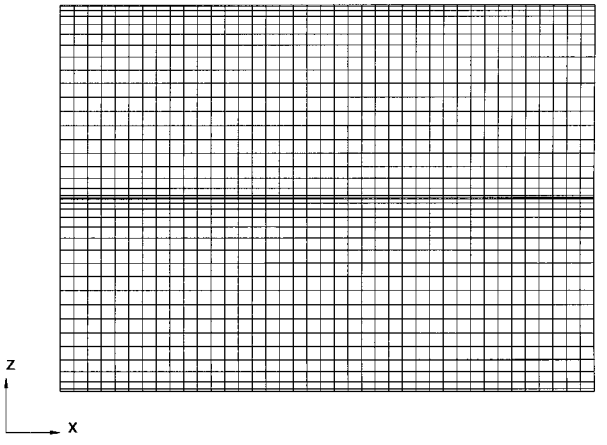

Figure 2. Cartesian mesh composed of two subgrids discretizing media I and II. The vertical grid points correspond to the collocations points of a modified Chebyshev differential operator. The non-periodicity of this operator allows the implementation of general boundary conditions at the horizontal boundaries. In the horizontal direction, a periodic Fourier differential operator is used

where ζ_i are the Gauss–Lobato collocation points, and g is a grid stretching function that stretches the super fine Chebyshev grid near the boundaries to have a minimum grid size of the order of the desired time step. Then, vertical derivatives are calculated by the chain rule

$$\frac{\partial f}{\partial z} = \frac{\partial f}{\partial \zeta}\frac{\partial \zeta}{\partial z} \tag{8}$$

The derivative with respect to ζ at the ith sampling point is

$$\frac{\partial f}{\partial \zeta}(\zeta_i) = \sum_{k=1}^{N_z - 1} b_k Q_k(\zeta_i), \quad i = 0, \ldots, N_z - 1 \tag{9}$$

where Q_k are Chebyshev polynomials, and b_k are the coefficients for the derivatives.[13]

The reason for using the Fourier and Chebyshev methods for computing the spatial derivatives is that these differential operators are infinitely accurate up to the Nyquist wave number of the mesh, that corresponds to a spatial wavelength of two grid points (at maximum spacing for the Chebyshev operator). This fact makes these so-called pseudospectral methods very efficient in terms of computer storage and the Chebyshev technique highly accurate for simulating Neumann and Dirichlet boundary conditions. The advantages over finite difference and finite element techniques lie in the absence of any numerical dispersion and in the use of a smaller number of grid points. These facts make the algorithm highly accurate and computationally efficient.

More details about the numerical technique can be found, for instance, in Carcione.[8]

3. SIMULATIONS

The transversely isotropic medium is defined by the elastic constants $c_{11} = 12{\cdot}5$ GPa, $c_{13} = 1$ GPa, $c_{33} = 8$ GPa and $c_{55} = 2{\cdot}88$ GPa, and the density $\rho = 2000\,\mathrm{kg/m^3}$. The corresponding horizontal and vertical compressional velocities are 2500 and 2000 m/s, respectively, while the associated shear velocity is 1200 m/s. For illustration, Figure 3 shows a polar representation of the energy (group) velocity corresponding to the qP (quasi-compressional) and qS (quasi-shear) waves, where the vertical axis is the symmetry axis perpendicular to the plane of isotropy (by symmetry considerations, only one quarter of the plane is displayed). The crack is located at 14·6 cm from the surface and has an extension of 14·4 cm. At the sides of the crack, the choice $\kappa_i \to 0$ and $\zeta_i \to \infty$ gives a welded interface, simulating a homogeneous medium. Note that these boundary conditions do not model a crack in the traditional sense of the term since they do not account for the $1/\sqrt{r}$ stress singularity at the crack tip. Such a model would require a displacement discontinuity proportional to the corresponding stress times the radial distance to the crack tip [10]. In this way, zero opening at the tips can be simulated. A uniformly distributed vertical load with a Ricker wavelet time-history of central frequency $f_0 = 110$ kHz is applied at the surface. The load consists of discrete delta functions applied on the first row of the mesh, between grid points 132 and 242.

We consider four cases whose crack properties are given in Table I. Also, the amount of dissipation, energy reflection coefficient and phase change at the crack surface for a normal incidence compressional plane wave of angular frequency $\omega_0 = 2\pi f_0$ are illustrated. These quantities are evaluated in Appendix I by means of a plane wave analysis. In case 1, the crack surface satisfies stress-free boundary conditions. In case 4, $\omega_P/\omega = 1$ and ζ_x and ζ_z are given by

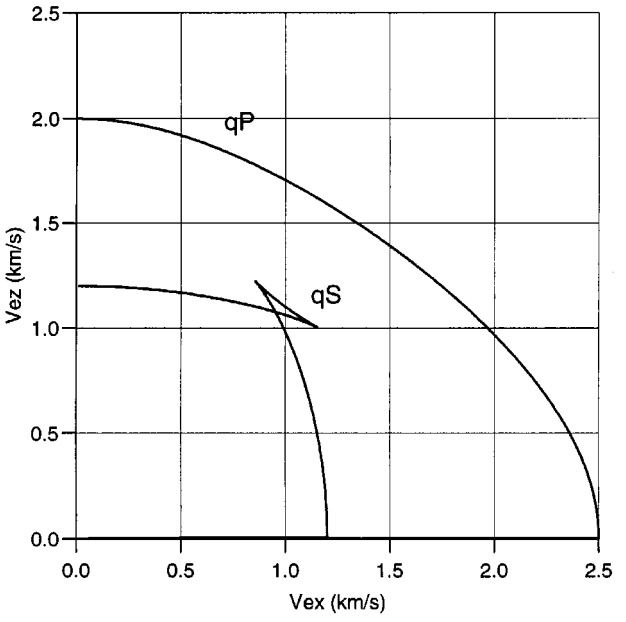

Figure 3. Polar representation of the energy velocity curves corresponding to the qP and qS wave modes. Due to symmetry, only one quarter of the curves are represented

Table I. Crack properties

Case	κ_x	κ_z	ζ_x	ζ_z	Remarks
1	0	0	0	0	No dissipation, $\lvert R_{PP}\rvert^2 = 1$, no phase change
2	0	0	$Z_S/2$	$Z_P/2$	50% dissipation, $\lvert R_{PP}\rvert^2 = 0{\cdot}25$, no phase change
3	$\omega_0 Z_s/2$	$\omega_0 Z_P/2$	$Z_S/100$	$Z_P/100$	Negligible dissipation, $\lvert R_{PP}\rvert^2 \approx 0{\cdot}5$, 45° phase change
4	$\omega_0 Z_S/2$	$\omega_0 Z_P/2$	$Z_S/\sqrt{2}$	$Z_P/\sqrt{2}$	41% dissipation, $\lvert R_{PP}\rvert^2 \approx 0.14$, 22·5° phase change

equations (23) and (22), respectively. These choices imply a reflection coefficient

$$R_{PP} = (1 + \sqrt{2} + \imath)^{-1} \tag{10}$$

for a normal incidence compressional wave of frequency f_0 [see equation (16)].

Figure 4 represents the normal incidence reflection and transmission coefficients $|R_{PP}|$ and $|T_{PP}|$ versus the normalized specific viscosity ζ_z/Z_P, corresponding to case 4. The limit $\zeta_z \to \infty$

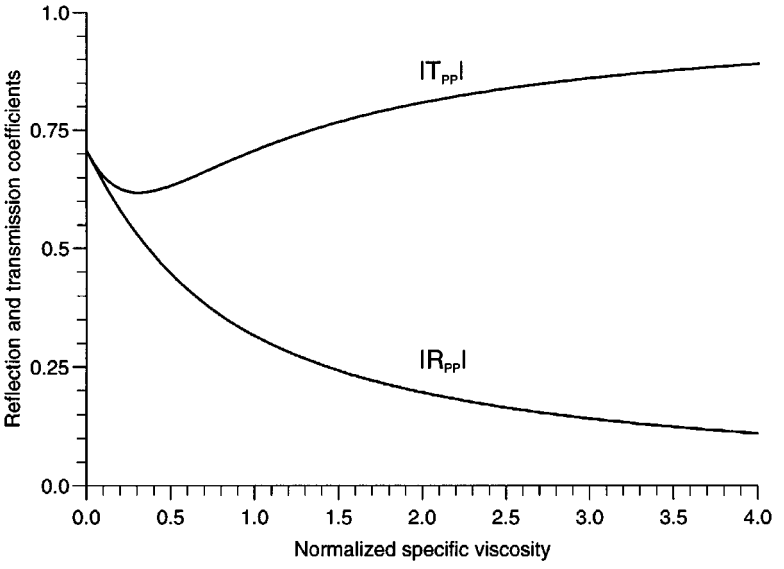

Figure 4. Normal incidence reflection and transmission coefficients $|R_{PP}|$ and $|T_{PP}|$ versus normalized specific viscosity ζ_z/Z_P, corresponding to case 4 of Table I

gives the welded interface, since $R_{PP} \to 0.$ and $T_{PP} \to 1$. The normalized energy loss for an incident compressional plane wave is represented in Figure 5, where it is confirmed that the maximum dissipation occurs for $\zeta_z = Z_P/\sqrt{2}$, the value given it the table and predicted by equation (22). Similar plots and conclusions are obtained for an incident S wave, for which the maximum loss occurs when $\zeta_x = Z_S/\sqrt{2}$. Moreover, it can be shown that, for any incident angle and values of the specific stiffnesses, there is no energy loss when $\zeta_z \to 0$ and $\zeta_z \to \infty$.

The calculations use two meshes with $N_x = 375$ and $N_z = 81$ each, and a horizontal grid spacing $D_x = 2\,\text{mm}$. The vertical load is applied from grid point 132 to grid point 242, and has a length of 22 cm. The upper boundary of the model (mesh 1) has stress-free conditions. The details about the differential operators used to compute the spatial derivatives can be found, for instance, in Carcione.[8] The solution is propagated to 0·136 ms with a time step of 0·1 μs, by using a fourth-order Runge–Kutta integration scheme.

Snapshots of the v_x and v_z components, at a propagation time of 136 μs, are illustrated in Figures 6–9. The different waves are identified by labels in Figure 6. For visual reasons, the v_x snapshots are enhanced a factor 5 with respect to the v_z snapshots. The leading pulse is the compressional wave, that is followed by the shear wave. Moreover, it is clear how the crack tips act as secondary sources, producing body waves (compare the wavefronts to the energy velocity plots of Figure 3). At the surface, the shear waves are followed by Rayleigh pulses originated at the load edges. Rayleigh waves can also be observed at the crack interface in Figure 6, that satisfies stress-free boundary conditions (the crack completely reflects the incident wave). Then, case 3 presents the stronger reflected wave and, in cases 2 and 4, the scattered fields are weaker due to energy loss at the crack surface (compare, for instance, the v_x components). These phenomena are in agreement with the theoretical predictions summarized in Table I. The wraparound effects

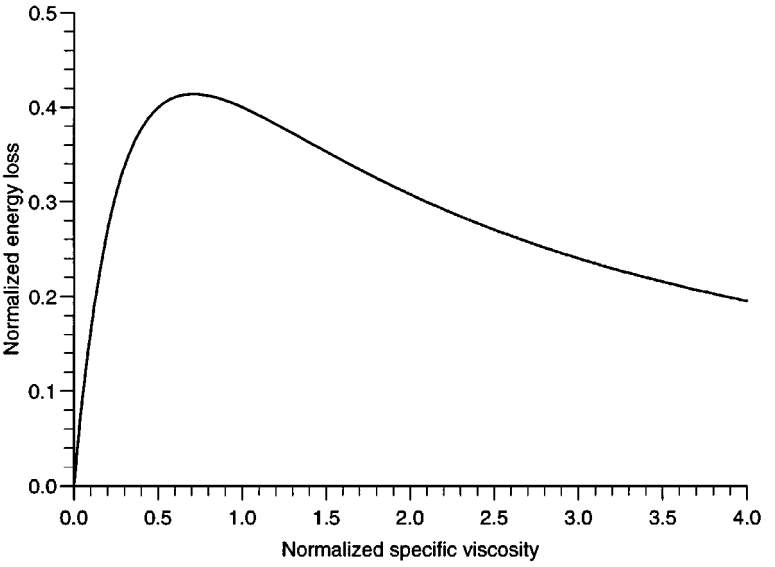

Figure 5. Normalized energy loss $\varepsilon_{\text{loss}}$ versus normalized specific viscosity ζ_z/Z_P, corresponding to case 4 of Table I

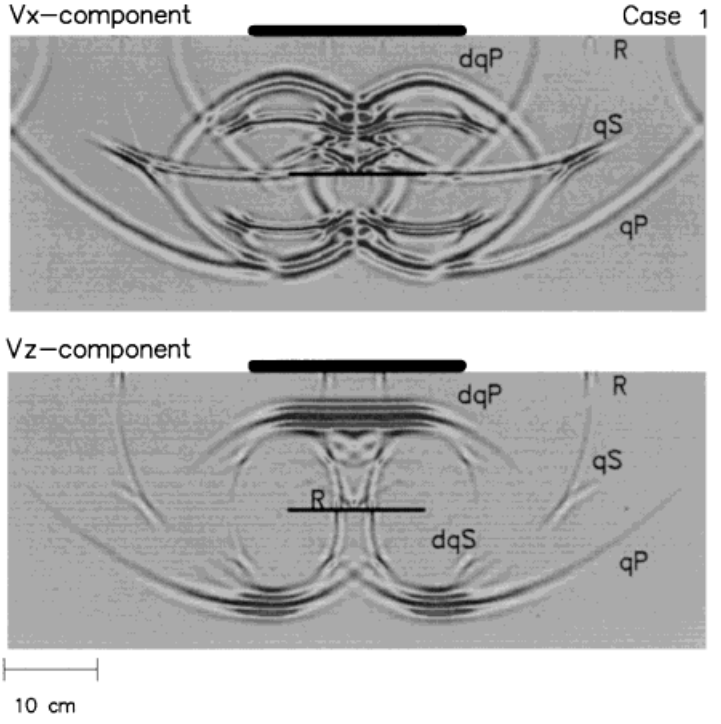

Figure 6. Vertical surface load radiation and crack scattering for case 1 of Table I. The snapshots show the v_x and v_z components at a propagation time of 136 μs. The labels identify the different waves: qP is the incident quasi-compressional wave, qS is the incident quasi-shear wave, R denotes the Rayleigh waves and $dq\,P$ and $dq\,S$ are the diffracted body waves

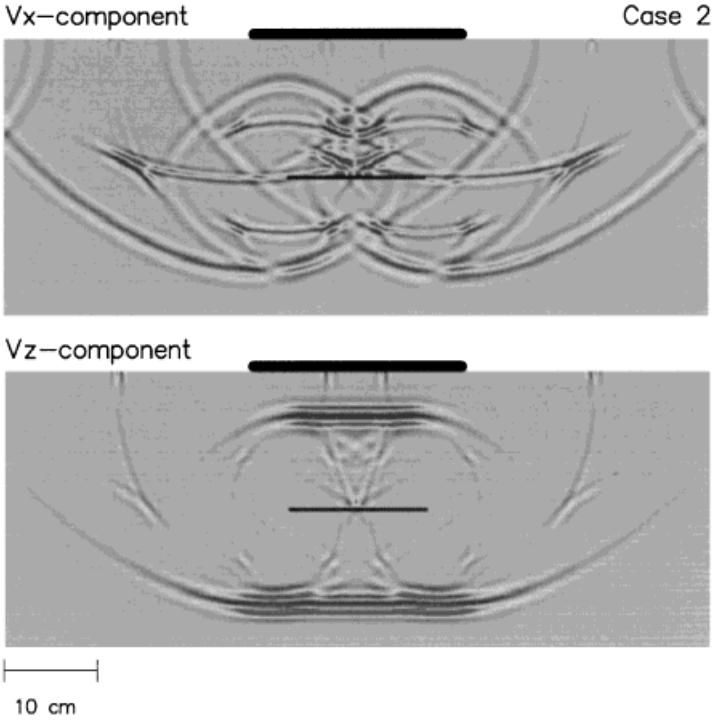

Figure 7. Vertical surface load radiation and crack scattering for case 2 of Table I. The snapshots show the v_x and v_z components at a propagation time of 136 μs.

observed at the sides, mainly in the v_x component, are caused by the periodicity of the Fourier differential operator.

4. CONCLUSIONS

The proposed numerical simulation technique is used to compute the elastic wave scattering produced by a crack embedded in a transversely isotropic medium. The crack surface satisfies quite general boundary conditions, from welded contact to a stress-free interface. The theory allows frequency-dependent reflection and transmission coefficients, phase changes and energy dissipation.

The numerical method for solving wave propagation uses a domain decomposition technique, that assigns a different mesh to each side of the interface. The use of the Chebyshev differential operator, to compute the spatial derivatives normal to the interface, allows the imposition of general boundary conditions. In particular, a boundary treatment, based on characteristic variables, implements the interface model in the velocity–stress formulation of the wave equation. The method allows complete material variability at any point of the model space. The examples show how the modelling algorithm correctly simulates the influence of the non-ideal interface on the different waves, in particular, tip diffractions, interface waves, partial reflection and transmission, and energy dissipation. The modelling algorithm can be used, for instance, to investigate the propagation of interface waves along cracks and fractures.[11, 12]

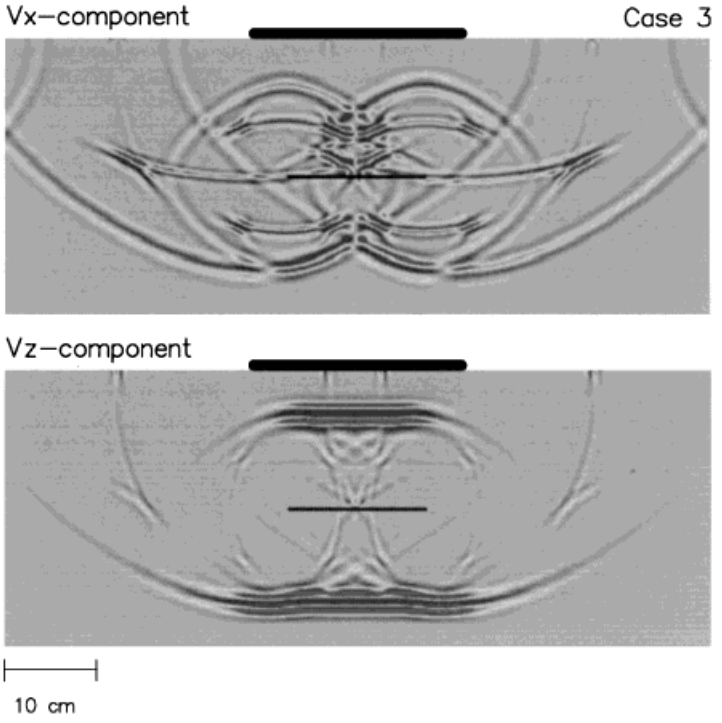

Figure 8. Vertical surface load radiation and crack scattering for case 3 of Table I. The snapshots show the v_x and v_z components at a propagation time of 136 μs.

Further developments of the method will allow, for instance: the treatment of cracks of arbitrary shape by co-ordinate mapping transformations; and axisymmetric scattering by a circular crack, that requires the use of cylindrical co-ordinates and a slight modification of the 2-D cartesian code.

ACKNOWLEDGEMENTS

This work was funded in part by AGIP S.p.A. and the European Commission in the framework of the JOULE programme, sub-programme Advanced Fuel Technologies. I thank an anonymous reviewer for the many comments and suggestions.

APPENDIX I. PLANE WAVE ANALYSIS FOR NORMAL INCIDENCE

Consider that the crack surface separates two media with equal material properties, and that the boundary conditions are given by (1)–(4). Since the crack surface is perpendicular to the symmetry axis of the transversely isotropic medium, the normal to that surface represents a pure mode direction. Then, the compressional and shear waves are decoupled and the problem of transmission and reflection can be treated separatedly.

Assume an incident compressional plane wave of the form

$$u_z)_I = \exp[\imath(k_p z - \omega t)] \tag{11}$$

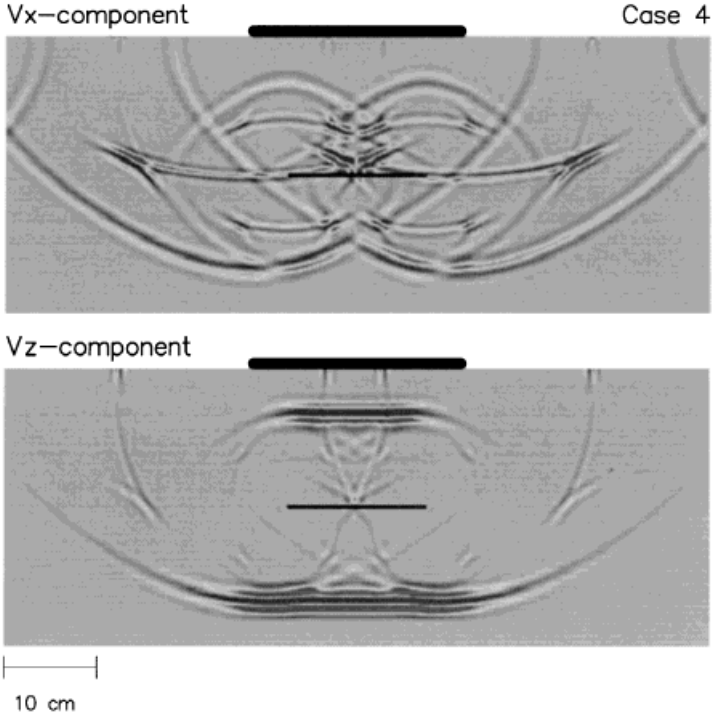

Figure 9. Vertical surface load radiation and crack scattering for case 4 of Table I. The snapshots show the v_x and v_z components at a propagation time of 136 μs

where $\imath = \sqrt{-1}$, ω is the angular frequency and $k_p = \omega\rho/Z_p$, with $Z_P = \sqrt{c_{33}\rho}$, c_{33} the elastic constant along the direction normal to the crack plane and ρ the material density. Then, the reflected and transmitted waves can be written as

$$u_z)_R = R_{PP}\exp[-\imath(k_P z + \omega t)] \tag{12}$$

$$u_z)_T = T_{PP}\exp[\imath(k_P z - \omega t)] \tag{13}$$

Substituting the displacements (11)–(13) into (2) and (4) and using $[v_z] = \imath\omega[u_z]$, gives

$$(T_{PP} - 1 - R_{PP})(\kappa_z - \imath\omega\zeta_z) = \imath k_P c_{33} T_{PP} \tag{14}$$

$$\imath k_P c_{33} T_{PP} = \imath k_p c_{33}(1 - R_{PP}) \tag{15}$$

respectively. Use of $k_P = \omega\rho/Z_P$ and after some algebra, yields the expressions for the reflection and transmission coefficients are

$$R_{PP} = \left(1 + \imath\frac{\omega_P}{\omega} + 2\frac{\zeta_z}{Z_P}\right)^{-1} \tag{16}$$

$$T_{PP} = 1 - R_{PP} \tag{17}$$

where $\omega_P = 2\kappa_z/Z_p$ is the characteristic frequency that defines the transition from an apparently perfect interface to the apparently decoupled one.[14] If $\kappa_z = 0$, then $\omega_P = 0$ and the particle velocity discontinuity model is obtained. In this case, the coefficients are frequency independent and there are no phase changes. On the other hand, when $\zeta_z = 0$, the theory gives the displacement discontinuity model. It is shown below that a discontinuity in the particle velocity implies energy dissipation at the interface.

Moreover, if $\zeta_z \to 0$ and $\kappa_z \to 0$, $R_{PP} \to 1$ and $T_{PP} \to 0$, and the free surface condition is obtained; when $\zeta_z \to \infty$, $R_{PP} \to 0$ and $T_{PP} \to 1$, giving the solution for a welded contact.

The reflection and transmission coefficients corresponding to an incident S wave can be obtained in the same way as for the incident P wave. In particular, the normal incident coefficients R_{SS} and T_{SS} have the same form as (16) and (17) but substituting κ_z by κ_x and ζ_z and ζ_x.

The normal component of the mean energy flux is continuous at a welded interface. This is a consequence of the boundary conditions that impose continuity of normal stress and particle velocity. For a normal incidence compressional wave, the normal component of the mean energy flux is proportional to the real part of $\sigma_{zz}v_z^*$, where the symbol $*$ denotes complex conjugate. However, at a non-welded interface, the discontinuity of the particle velocity implies that the energy flux is also discontinuous. The difference between the sum of the reflected and transmitted energies and the incident energy is the energy dissipated at the interface.

After normalizing with respect to the incident wave, the reflected and transmitted energy fluxes are

$$\text{reflected} \quad P \text{ wave} \to |R_{PP}|^2 \tag{18}$$

$$\text{transmitted} \quad P \text{ wave} \to |T_{PP}|^2 \tag{19}$$

Hence, the normalized dissipated energy is

$$\varepsilon_{\text{loss}} = 1 - |R_{PP}|^2 - |T_{PP}|^2 \tag{20}$$

Substituting (17), the energy loss becomes

$$\varepsilon_{\text{loss}} = \frac{4\zeta_z/Z_P}{(1 + 2\zeta_z/Z_P)^2 + (\omega_P/\omega)^2} \tag{21}$$

The displacement discontinuity model ($\zeta_z = 0$) yields no dissipation. On the other hand, the maximum loss is obtained for

$$\zeta_z = \frac{Z_P}{2}\sqrt{1 + \left(\frac{\omega_P}{\omega}\right)^2} \tag{22}$$

Similarly, the maximum loss for an incident S wave occurs for

$$\zeta_x = \frac{Z_S}{2}\sqrt{1 + \left(\frac{\omega_S}{\omega}\right)^2} \tag{23}$$

where $\omega_S = 2\kappa_x/Z_s$.

REFERENCES

1. L. J. Pyrak-Nolte, L. R. Myer, N. G. W. Cook, 'Transmission of seismic waves across single natural fractures', *J. Geophys. Res.*, **95,** 8617 (1990).

2. S. Crampin, R. McGonigle, D. Bamford, 'Estimating crack parameters from observations of P-wave velocity anisotropy', *Geophysics*, **45,** 345 (1980).
3. J. D. Achenbach, From ultrasonics to failure prevention, in S. K. Datta *et al*. ed., *Elastic Waves and Ultrasonic Nondestructive Evaluations*, 1990, Elsevier, Amsterdam, 1990, p. 217.
4. M. Schoenberg, 'Elastic wave behavior across linear slip interfaces', *J. Acoustic. Soc. Am*., **68,** 1516 (1980).
5. T. Kundu and A. Boström, 'Elastic wave scattering by a circular crack in a transversely isotropic solid', *Wave Motion*, **15,** 285 (1992).
6. Z. Mroz, and G. Giambianco, 'An interface model for analysis of deformation behaviour of discontinuities', *Int. J. Numer. Anal. Meth. Geomech.* **20,** 1–33 (1996).
7. J. M. Carcione, 'Domain decomposition for wave propagation problems', *J. Sci. Comput*., **6,** 453 (1991).
8. J. M. Carcione, 'Time-dependent boundary conditions for the 2-D linear anisotropic–viscoelastic wave equation', *Numer. Meth. Part. Diff. Equations*, **10,** 772 (1994).
9. E. Tessmer, D. Kessler, D. Kosloff and A. Behle, 'Multi-domain Chebyshev-Fourier method for the solution of the equations of motion of dynamic elasticity', *J. Comput. Phys*., **100,** 355 (1992).
10. P. A. Charlez, *Rock Mechanics*, *Vol. 1*, *Theoretical Fundamentals*, Editions Technip, 1991.
11. L. J. Pyrak-Nolte, J. Xu and G. M. Haley, 'Elastic interface waves propagating in a fracture', *Phys. Rev. Lett*. **68,** 3659–3653 (1992).
12. B. Gu, K. T. Nihei, L. R. Myer and L. J. Pyrak-Nolte, 'Fracture interface waves', *J. Geophys. Res*., **101,** 827–835 (1996).
13. D. Gottlieb and S. A. Orszag, 1977, Numerical analysis of spectral methods: Theory and applications, CBMS Reg. Conf. Series in Appl. Math. 26, Soc. Ind. and Appl. Math.
14. P. B. Nagy and L. Adler, 'New ultrasonic techniques to evaluate interfaces', in S. K. Datta *et al* (ed.), *Elastic Waves and Ultrasonic Nondestructive Evaluations*, 1990 (Elsevier, North-Holland, 1990), p. 229.

